

Entanglement Hamiltonian in the non-Hermitian SSH model

Federico Rottoli¹, Michele Fossati¹, and Pasquale Calabrese^{1,2}

¹*SISSA and INFN Sezione di Trieste, via Bonomea 265, 34136 Trieste, Italy.*

²*ICTP, Strada Costiera 11, 34151 Trieste, Italy.*

Abstract

Entanglement Hamiltonians provide the most comprehensive characterisation of entanglement in extended quantum systems. A key result in unitary quantum field theories is the Bisognano-Wichmann theorem, which establishes the locality of the entanglement Hamiltonian. In this work, our focus is on the non-Hermitian Su–Schrieffer–Heeger (SSH) chain. We study the entanglement Hamiltonian both in a gapped phase and at criticality. In the gapped phase we find that the lattice entanglement Hamiltonian is compatible with a lattice Bisognano-Wichmann result, with an entanglement temperature linear in the lattice index. At the critical point, we identify a new imaginary chemical potential term absent in unitary models. This operator is responsible for the negative entanglement entropy observed in the non-Hermitian SSH chain at criticality.

Contents

1	Introduction	2
2	The non-Hermitian Su–Schrieffer–Heeger model	4
2.1	<i>bc</i> -ghost CFT	5
2.2	Left-right ground-state	6
2.3	Correlation function	6
3	Lattice entanglement Hamiltonians of the non-Hermitian SSH model	7
3.1	Entanglement Hamiltonian in the trivial gapped phase	8
3.2	Entanglement Hamiltonian at the critical point	10
4	Conclusions	15

1 Introduction

In recent years, the study of entanglement has attracted a lot of interest from several different communities and has emerged as a unifying theme across quantum physics, in fields ranging from quantum information [1] and high energy physics [2], to statistical mechanics [3–5] and condensed matter physics [6]. Given a pure state described by the density matrix $\rho = |\Psi\rangle\langle\Psi|$ and considering a bipartition of the system in A and B , the information about the entanglement between the two subsystems is encoded in the reduced density matrix, obtained by tracing over the Hilbert space of one of the two subsystems

$$\rho_A = \text{Tr}_B \rho. \quad (1)$$

If the density matrix ρ is entangled, then the reduced density matrix in Eq. (1) corresponds a mixed state and the von Neumann and Rényi entropies of ρ_A [7, 8]

$$S_A = -\text{Tr}[\rho_A \log \rho_A], \quad S_A^{(n)} = \frac{1}{1-n} \log \text{Tr} \rho_A^n. \quad (2)$$

are good entanglement monotones. The knowledge of all the Rényi entropies allows in turn to compute the full entanglement spectrum, i.e, the spectrum of the reduced density matrix [9–11].

While the entanglement entropies in Eq. (2) are very useful, they do not entirely capture the entanglement properties of the system. Over the years, more comprehensive characterisations, beyond what can be exclusively derived from the knowledge of the entanglement spectrum, have been investigated. Arguably, the most complete understanding stems from the entanglement (or modular) Hamiltonian (EH), which is the logarithm of the (normalised) reduced density matrix [12–14]

$$\rho_A = \frac{e^{-K_A}}{Z_A}. \quad (3)$$

This operator contains much more information than the entanglement entropies, since, unlike the latter, its specific form depends not only on the eigenvalues but also on the eigenvectors of ρ_A .

Although calculating the EH is considerably more challenging than determining the entanglement entropies, a rich theoretical framework has been developed during the last decades. The most remarkable result is the Bisognano-Wichmann (BW) theorem [12–16]. Considering the vacuum state of a unitary relativistic quantum field theory (QFT) on \mathbb{R}^{d+1} and taking as subsystem the half-space $x^1 > 0$, the Bisognano-Wichmann theorem asserts that the entanglement Hamiltonian in the half-space is the generator of Lorentz boosts

$$K_A = 2\pi \int_{x^1 > 0} d^d x x^1 T_{00}(x), \quad (4)$$

where $T_{00}(x)$ is the energy density. This result is remarkable for several reasons. First, it is extremely general, holding for all unitary Lorentz invariant QFTs, independently of the dimension of space-time and of the mass spectrum. Another significant property is the fact that the BW Hamiltonian in Eq. (4) has a local structure, given by the integral of local operator with a linearly increasing local entanglement temperature $\beta(x) = x^1$. Finally, the Bisognano-Wichmann theorem provides a mathematical proof of the Unruh effect [17–19], as discussed in [12–14].

For generic massive QFTs, the Bisognano-Wichmann theorem in Eq. (4) is the only known analytic result. For conformal field theories (CFT), instead, the extended symmetry makes it possible to obtain more general results. In particular, the Hislop-Longo theorem [12, 20] (see also [21–23]) provides the entanglement Hamiltonian of the ground state of a CFT in any ball

shaped region. Even more general results can be obtained in 1 + 1-dimensional unitary CFTs, where the infinite dimensional Virasoro symmetry allows one to map the Bisognano-Wichmann result in Eq. (4) in several different geometries [22, 23]. In particular, for the conformal vacuum state, if the subsystem is a single interval ($A = [0, \ell]$) the entanglement Hamiltonian takes the form [20–23]

$$K_A = 2\pi \int_0^\ell dx \beta(x) T_{00}(x), \quad \text{with } \beta(x) = \frac{x(\ell - x)}{\ell}, \quad (5)$$

a formula that inherits the local structure of the Bisognano-Wichmann result, with a parabolic local entanglement temperature $\beta(x)$. We remark that this local structure is very peculiar and it fails to hold as soon as we consider minor modifications such as for the lowest excited states [24] and when considering multiple intervals [25, 26]. This property is not only of theoretical interest, but recently in Refs. [27–31] it has been leveraged to efficiently construct in synthetic quantum systems the ground state of lattice models using a variational approach.

A separate line of research, yielding numerous results, concerns the study of the EH in unitary 1 + 1-dimensional integrable lattice model [32–47]. In these systems, the entanglement Hamiltonian of the ground state in the half-space $x > 0$ is intimately related to Baxter’s corner transfer matrix (CTM) \widehat{A} [48–50]. Considering, for example, isotropic square lattices, the effect of the corner transfer matrix is to add a full angular segment to a piece of lattice, mapping a horizontal row to a vertical one and vice versa. Using this property it is possible to show that the lattice reduced density matrix in the half-line can be expressed as the product of four CTMs [7, 35, 51]

$$\rho_A = \frac{\widehat{A}^4}{\text{Tr } \widehat{A}^4}, \quad (6)$$

where $Z = \text{Tr } \widehat{A}^4$ is the partition function. Recalling the definition (3) of the entanglement Hamiltonian, Eq. (6) implies that it is proportional to the logarithm of fourth power of the corner transfer matrix [35]

$$K_A = -\log \widehat{A}^4. \quad (7)$$

This correspondence between entanglement Hamiltonians and CTMs has made it possible to obtain the EHs in several integrable models. It has been observed that in certain integrable models, the logarithm of the CTM and the EH can be written in terms of the density of the lattice Hamiltonian h_j with a linearly increasing local temperature

$$K_A \propto \sum_{j=0}^{\infty} j h_j, \quad (8)$$

with a non-trivial proportionality constant. This behaviour has been identified in various spin systems such as the Ising model [33–35], the XXZ [36, 37, 48], the XYZ chains [38–40], the anisotropic XX chain [43], and in bosonic models such as the harmonic chain [41–43]. Comparing Eq. (8) with the Bisognano-Wichmann theorem in Eq. (4), it is evident that the two entanglement Hamiltonians share the same structure. In fact, the connection between the two results runs deeper than a superficial similarity. Tetel’man [38] and Itoyama and Thacker [39, 52–54] independently showed that in these integrable models the logarithm of the corner transfer matrix is the generator of a continuous group of lattice Lorentz transformations, akin to the role played by the generator of Lorentz boosts in the BW theorem.

Despite the wealth of results for unitary models, nothing is known for non-Hermitian theories. In particular, since one of the hypothesis of the Bisognano-Wichmann theorem (4) is that the Hilbert space carries a unitary representation of the Poincaré group [12, 15, 16], it is not obvious how to adapt to non-unitary CFTs this theorem and its corollary (5). Non-Hermitian



Figure 1: Schematic representation of the nH-SSH model, described by Eq. (9). The nearest neighbours hoppings have alternating strengths v and w . The imaginary chemical potential is set to iu on the even sites and $-iu$ on the odd sites.

models [55, 56] have recently attracted a lot of interest for several reasons, including but not restricted to the study of the PT -symmetric systems [57–59], optical phenomena [60, 61] and the study of open systems [62–64] and measurement induced transitions [65–69]. It is then very natural to explore the entanglement properties within this class of systems.

A pioneering study was carried out in Ref. [70], where the authors have studied the entanglement entropy and the entanglement spectrum in the non-Hermitian Su-Schrieffer-Heeger (SSH) model at criticality (reviewed in Sec. 2). Remarkably, it was observed that the entanglement entropies obey the logarithmic dependence on the subsystem length typical of critical systems [7, 71], but with a negative central charge $c = -2$ (see also [72]). Later, in Ref. [73], the analysis has been extended to the symmetry resolved EEs. In this work we move a step further, conducting an exploratory and thorough numerical investigation of the entanglement Hamiltonian in the non-Hermitian Su-Schrieffer-Heeger model, both in the gapped phase and at criticality. In the gapped phase we observe that the lattice EH has a structure analogous to the one of integrable lattice models reported in Eq. (8). At the critical point, we instead find an additional term not accounted for in the Bisognano-Wichmann corollary in Eq. (5), which is responsible for the negativeness of the entanglement entropies.

The present manuscript is organised as follows. First, in Sec. 2 we review the non-Hermitian Su-Schrieffer-Heeger model, with particular focus on the non-unitary $c = -2$ bc -ghost CFT which describes the critical point. In Sec. 3 we report the main results of this work, the numerical lattice entanglement Hamiltonian in the non-Hermitian SSH model. We first consider the topologically trivial gapped phase in Sec. 3.1 and we then study the critical point in Sec. 3.2. We draw our conclusions in Sec. 4.

2 The non-Hermitian Su–Schrieffer–Heeger model

Before presenting our results, in this section we review the non-Hermitian model that we study in this paper. We consider the non-Hermitian SSH (nH-SSH) chain with PT -symmetry on a discrete circle of $L = 2N$ sites, described by the Hamiltonian

$$H = \sum_{j \in \mathbb{Z}_N} \left(-w c_{2j}^\dagger c_{2j+1} - v c_{2j-1}^\dagger c_{2j} + \text{h.c.} \right) + iu \sum_{j \in \mathbb{Z}_N} \left(c_{2j}^\dagger c_{2j} - c_{2j+1}^\dagger c_{2j+1} \right), \quad (9)$$

with $u, v, w > 0$. A schematic representation of this Hamiltonian is depicted in Fig. 1. We assume quasi-periodic boundary conditions, i.e., $c_{j+L} = e^{i\delta} c_j$, with $0 < \delta \ll 1$. The reason for this choice will be explained later. The model is a fermionic chain with nearest neighbours hoppings, which have alternating strength on even-odd links. The staggered imaginary chemical potential breaks the hermiticity of the Hamiltonian. Notice that our conventions match those in Ref. [72] after setting $v_1 = 0$ and $v_2 = v$ and identifying their up (down) sites with our even (odd) ones.

The Hamiltonian becomes block diagonal after a Fourier transform of the lattice operators, performed separately on the even and odd sites

$$\tilde{c}_{k,e} = \frac{1}{\sqrt{N}} \sum_{j \in \mathbb{Z}_N} e^{-ikj} c_{2j}, \quad \tilde{c}_{k,o} = \frac{1}{\sqrt{N}} \sum_{j \in \mathbb{Z}_N} e^{-ikj} c_{2j+1}, \quad (10)$$

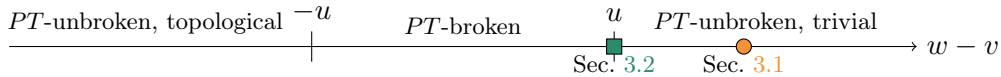


Figure 2: Phase diagram of the nH-SSH model, explained in the main text. The orange circle and the green square mark the points in parameter space for which we study the entanglement Hamiltonian, reported in Sec. 3.1 and Sec. 3.2 respectively.

with

$$k \in \frac{2\pi}{N} \left(\mathbb{Z}_N + \frac{\delta}{2\pi} \right), \quad (11)$$

where the shift in momentum space is due to the δ -twisted boundary conditions. The Hamiltonian then becomes

$$H = \sum_k \begin{pmatrix} \tilde{c}_{k,e}^\dagger & \tilde{c}_{k,o}^\dagger \end{pmatrix} \begin{pmatrix} iu & -w - ve^{-ik} \\ -w - ve^{ik} & -iu \end{pmatrix} \begin{pmatrix} \tilde{c}_{k,e} \\ \tilde{c}_{k,o} \end{pmatrix}, \quad (12)$$

and the eigenvalues of the matrix in Eq. (12) are the single particle energies.

Varying the relative strengths of the parameters u, v, w , the model admits three different gapped phases [70]. If $v - w \in (-u, u)$, the PT symmetry is broken so that the energy spectrum is complex and the eigenvalues appear in complex conjugate pairs. In the two phases $v - w > u$ or $v - w < -u$, the PT symmetry is unbroken and the energy spectrum is real. The latter two phases are distinguished by topological properties, as discussed in [74]. The resulting phase diagram is given in Fig. 2.

Two critical points occur for $v - w = \pm u$. In these cases, the single particle spectrum is $\epsilon_{\pm,k} = \pm\sqrt{2vw(1 + \cos k)}$ and the gap closes at $k = \pi$, leading locally to a linear spectrum with speed of sound

$$c_S = \sqrt{vw}. \quad (13)$$

Moreover, at $k = \pi$ the kernel of the Hamiltonian (12) is not diagonalisable, as it is made of a 2×2 Jordan block. This is called an exceptional point in momentum space. The exceptional point occurs because, as $k \rightarrow \pi$, the two eigenspaces become more and more collinear, and they perfectly coincide at $k = \pi$.

Finally, since the Hamiltonian is a linear combination of terms of the form $c_i^\dagger c_j$, it is invariant under the $U(1)$ generated by

$$Q = \sum_{j \in \mathbb{Z}_{2N}} c_j^\dagger c_j. \quad (14)$$

In this paper, we will investigate the ground-state of the system in the PT -unbroken trivial phase and the critical point between the PT -unbroken trivial phase and the PT -broken phase, marked in Fig. 2 with a orange circle and a green square, respectively. In [70], the latter point has been identified with the fermionic bc -ghost CFT with central charge $c = -2$, which we review in the following section.

2.1 bc -ghost CFT

The bc -ghost conformal field theories are a family of CFTs governed by the following action [75–79]

$$S = \int d^2z (b \bar{\partial} c + \bar{b} \partial \bar{c}), \quad (15)$$

where b and c are anticommuting holomorphic fields and \bar{b} and \bar{c} are the corresponding anti-holomorphic fields. The different members of this family are distinguished by the value of the

central charge and by the conformal dimension of the fields c and b . In particular, the CFT which describes the nH-SSH critical point is the one with central charge $c = -2$ [70], in which the fields have conformal weight $h_b = 1, h_c = 0$. All these theories have a conserved current $J = :cb:$ so that the field c has charge 1 and b has charge -1 , independently of the specific realisation and central charge.

The conformal field theory with $c = -2$ is one of the simplest instances of a logarithmic CFT [77], incorporating reducible but not indecomposable representations of the Virasoro algebra. Specifically, the fields c and the identity field share the same conformal weights, leading to the formation of a 2-dimensional Jordan block in the Virasoro modes L_0 and \bar{L}_0 . This phenomenon occurs exclusively in the untwisted sector of the theory, which corresponds to periodic boundary conditions on a cylinder. In the scenario where δ -twisted boundary conditions are adopted, the fields acquire a phase factor $e^{i2\pi\delta}$ as they move around the non-contractible loop of the cylinder. Consequently, the identity field is no longer part of the spectrum, and the system's ground state becomes associated with the twist field σ_δ [77]. The conformal dimension of σ_δ is given by $h_{\sigma_\delta} = \delta(\delta - 1)/2$, which is negative for $\delta \neq 0$. This implies that for $\delta \neq 0$, there is no Jordan block for L_0 and \bar{L}_0 , effectively eliminating the logarithmic singularities. It is noteworthy that the presence of the Jordan block in periodic boundary conditions and its absence in the twisted sectors draws a further analogy with the nH-SSH model.

2.2 Left-right ground-state

Before concluding this brief review, we would like to emphasise the states that are the focus of this paper. First, in both of the cases we consider (see Fig. 2), the Hamiltonian has a real spectrum, thus there is a well defined notion of a ground state as the eigenstate with minimum energy eigenvalue. We denote by $|R\rangle$ the right ground state of the Hamiltonian, defined by $H|R\rangle = E_{gs}|R\rangle$, while we denote with $\langle L|$ the left ground-state, defined by $\langle L|H = E_{gs}\langle L|$. Since the Hamiltonian is non-Hermitian, the left ground state is not the ‘‘bra’’ of the right ground state, in other words, $\langle L| \neq |R\rangle$.

We consider the density matrix $\rho = |R\rangle\langle L|$, which we call the left-right ground state [70, 72, 73, 80–84]. Indeed, this can be seen as the zero-temperature limit of the thermal state $e^{-\beta H}/Z$ and therefore is the most natural object to be studied in field theory. The density matrix ρ is positive semi-definite but not Hermitian and therefore the reduced density matrix ρ_A is not positive semi-definite. This means that the entanglement entropy between a subsystem and its complement can be negative. Indeed, the entanglement entropy scales as $c/3 \log \ell$, with $c = -2$ [70].

The symmetry-resolved entanglement, relative to the $U(1)$ symmetry (14), at the critical point has been studied in [73]. Of relevance for this paper, it has been understood that the eigenvalues of the reduced density matrix are either positive or negative depending on the sign of the charge sector, namely $\text{sign } \lambda_q = (-1)^{q-\langle Q_A \rangle}$, where λ_q stands for an eigenvalue of ρ_A in the charge sector q of Q_A (i.e. the charge (14) restricted to A). We will show in Sec. 3.2 that we can identify the source of this behaviour in the form of the entanglement Hamiltonian.

2.3 Correlation function

A key object in the analysis of the entanglement Hamiltonian of the left-right ground state is the two-point correlation matrix C with entries [70, 73]

$$C_{2j+a, 2l+b} = \langle L|c_{2j+a}^\dagger c_{2l+b}|R\rangle = \frac{1}{N} \sum_k e^{-ik(j-l)} \mathcal{G}(k)_{ab}, \quad a, b \in \{0, 1\}, \quad (16)$$

with

$$\mathcal{G}(k) = \frac{1}{2} \begin{pmatrix} 1 - \cos(2\xi_k) & -\sqrt{\frac{\eta_k^*}{\eta_k}} \sin(2\xi_k) \\ -\sqrt{\frac{\eta_k}{\eta_k^*}} \sin(2\xi_k) & 1 + \cos(2\xi_k) \end{pmatrix}, \quad (17)$$

where $2\xi_k = \tan^{-1}(|\eta_k|/(iu))$, $\eta_k = -w - ve^{-ik}$. Due to the dimerization of the hopping amplitudes v, w , the correlation matrix C presents a block structure. In the thermodynamic limit $L \rightarrow \infty$, C is a block Toeplitz matrix generated by the symbol \mathcal{G} .

3 Lattice entanglement Hamiltonians of the non-Hermitian SSH model

This section contains the main results of this paper, the numerical lattice entanglement Hamiltonian in the non-Hermitian SSH model and an analytic conjecture for its behaviour. In order to compute numerically the lattice EH we use the known relation between fermionic Gaussian states and the correlation matrix. Notice first that since the Hamiltonian (9) is quadratic, the ground state is Gaussian [70, 73] and the reduced density matrix can be written as

$$\rho_A = \frac{1}{Z_A} \exp \left\{ - \sum_{i,j \in A} c_i^\dagger k_{ij}^A c_j \right\}, \quad (18)$$

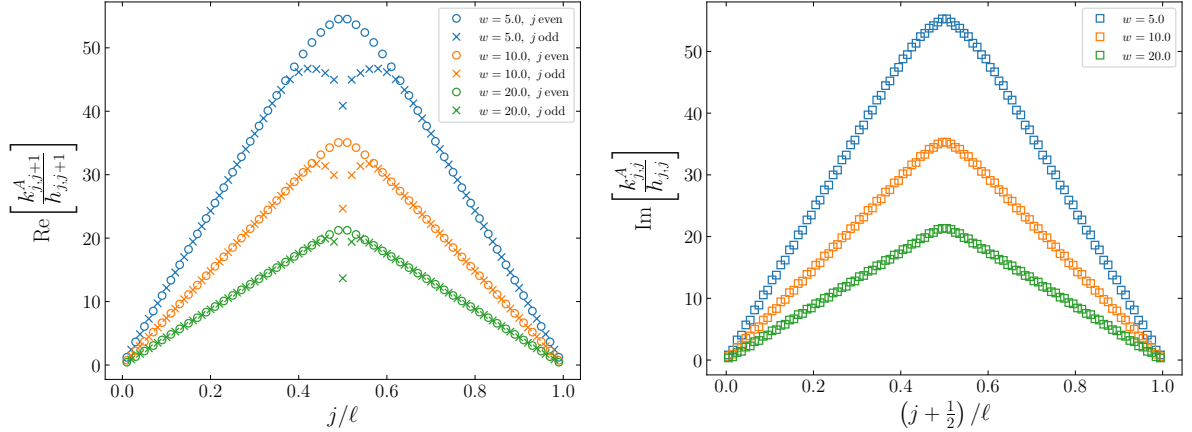
where k_{ij}^A is the kernel of the EH, i.e., the single particle entanglement Hamiltonian. For Gaussian states as in Eq. (18), the kernel k^A can be obtained from the knowledge of the reduced correlation matrix, i.e. the matrix (16) with indexes restricted to A , $(C_A)_{ij} = (C)_{i,j \in A}$. Using Peschel's formula [85–87] one has

$$k^A = \log [C_A^{-1} - \mathbb{I}]^T, \quad (19)$$

where T denotes the matrix transpose. While Eq. (19) was initially derived for Hermitian models, as discussed in Refs. [70, 73], it remains valid in the non-Hermitian one under consideration. In Refs. [70, 73] the restricted correlation matrix of the non-Hermitian SSH model is used for the computation of the entanglement spectrum and the entropies. In the following we will compute the kernel of the entanglement Hamiltonian using the correlation matrix (16).

We remark that the numerical computation of the formula (19) suffers from numerical instabilities and must be conducted at high precision. The reason for this instability is that many eigenvalues of the correlation matrix C_A are arbitrarily close to 0 and 1, and as a consequence the matrix inside of the logarithm in Eq. (19) has eigenvalues which are very close to 0 or very large. In our study we used the `python` library `mpmath` [88] and the software `Mathematica`, keeping up to 500 digits.

In rest of this section, we present the results for the entanglement Hamiltonian of an interval $A = [0, \ell]$ in the left-right ground state. We first study the topologically trivial gapped phase $w - v > u$ with periodic boundary conditions and we compare with the known results in unitary integrable lattice models [43]. We then consider the critical point $w - v = u$ with a small twisting of the boundary conditions $\delta = 10^{-7}$, which as we explained in Sec. 2 is described by the $c = -2$ bc -ghost CFT. We compare the results with the continuum prediction from unitary CFTs and we use our observations to formulate a conjecture for the entanglement Hamiltonian of an interval in the ground state of the bc -ghost theory.



(a) Real part of the nearest-neighbour coupling $k_{j,j+1}^A$. (b) Imaginary part of the chemical potential $k_{j,j}^A$.

Figure 3: Entanglement temperature in the gapped phase $w - v > u$. In both plots we fix $v = u = 1$ and we consider different values of $w = 5, 10$ and 20 and we take a subsystem of length $\ell = 100$ in a full system of total length $L = 2000$. In the left plot we report, as a function of j/ℓ , the real part of the ratio of the nearest-neighbour EH coupling $k_{j,j+1}^A$ with the coupling $(h_{j,j+1})$, i.e. $-w$ for even j (circles) and $-v$ for odd j (crosses). The purpose of this ratio is to isolate the entanglement temperature. Apart from a small region in the center of the interval, the ratio follows the expected triangular shape (see discussion below Eq. (20)). In the right plot we report the imaginary part of the ratio between the staggered imaginary chemical potential $k_{j,j}^A$ with $+u$ ($-u$) for even (odd) site j . Again, up to a small finite size oscillation, the ratio follows the predicted triangular shape.

3.1 Entanglement Hamiltonian in the trivial gapped phase

Before studying the non-Hermitian model, it is instructive to first recall the known results in unitary gapped lattice models, in order to compare them with ours. As we reported in Eq. (8) in Sec. 1, in certain integrable models the entanglement Hamiltonian in the half-space follows the structure recognised by Tetel'man, Itoyama and Thacker, i.e., the EH is proportional to the Hamiltonian density with a local temperature equal to the lattice site, analogous to a lattice Bisognano-Wichmann behaviour [14, 38, 39, 49, 50, 52]. If we instead consider a finite interval, in the general case there are very few known analytic results. If the gap is sufficiently large, however, in Ref. [43] it was observed via numerical computations that near the two endpoints of the interval the EH follows the half-space result of Eq. (8), only deviating from this behaviour in the middle of the interval, which give rise to a characteristic triangular entanglement temperature. This triangular behaviour has been observed in several Hermitian models, such as the Hermitian Su-Schrieffer-Heeger model (or dimerised hopping chain) and the harmonic chain [43]. It is arguably a straightforward consequence of cluster decomposition, which is independent of unitarity. It is therefore natural to wonder if this factorisation holds also for the non-Hermitian model under study. Another important consequence of Eq. (8) is that in unitary lattice integrable models, the half-space lattice EH does not couple fermions at distances larger than those in the corresponding lattice Hamiltonian. Correspondingly, within an interval, it was noted that near the endpoints, the entanglement Hamiltonian does not exhibit higher couplings, only manifesting them in the crossover region at the center [43].

Let us now consider the non-Hermitian SSH model. Assuming that the structure of the entanglement Hamiltonian in Eq. (8) holds also for this theory, from the Hamiltonian in Eq. (9)

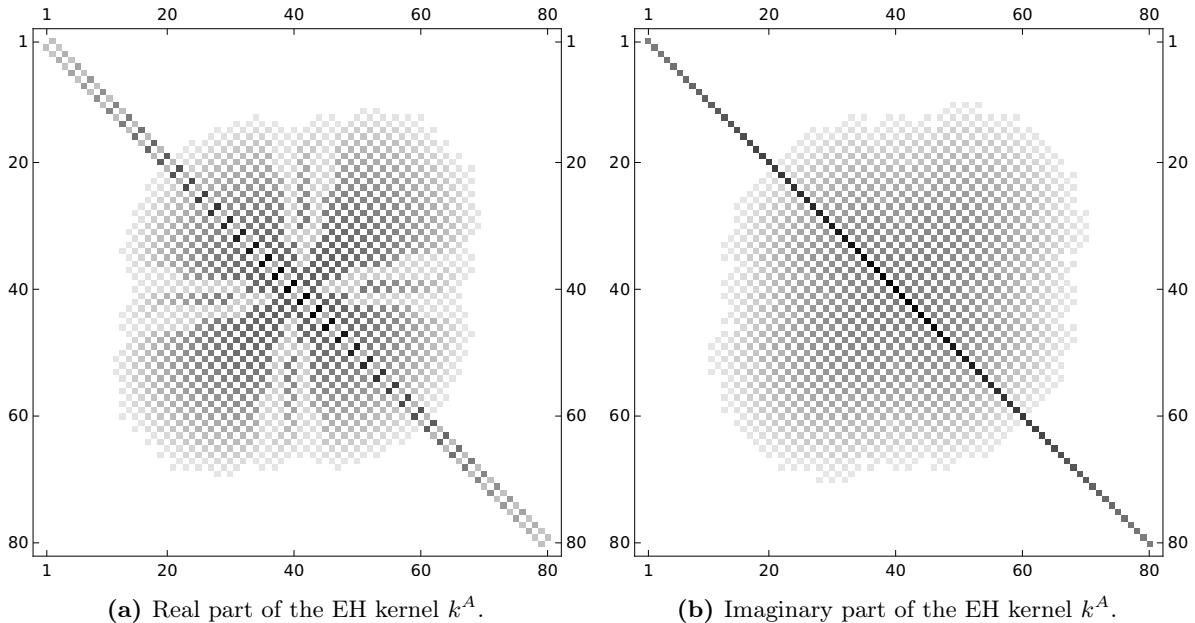


Figure 4: Matrix plot of the entanglement Hamiltonian kernel k^A in the gapped phase $w - v > u$ with $w = 20$, $v = 2$ and $u = 2$, for an interval of length $\ell = 80$ in a system of length $L = 2000$. Left (Right): Absolute value of the real (imaginary) part of k^A . Consistently with the Tetel'man-Thacker behaviour (20), near the two endpoints the only non-vanishing elements of the entanglement Hamiltonian are the imaginary chemical potential (main diagonal in the right plot) and the coupling between nearest-neighbours (first sub-diagonals in the left plots). The latter couplings (left) display the alternating value between the odd and even sites (see Eq. (20)). In the middle of the interval, the entanglement Hamiltonian deviates from Eq. (20) and also couplings at higher distances are non-zero.

we can conjecture that the half-space lattice EH takes the form

$$\begin{aligned}
 K_A \propto \sum_{j=0}^{+\infty} \left[(2j) w \left(c_{2j}^\dagger c_{2j+1} + c_{2j+1}^\dagger c_{2j} \right) + (2j+1) v \left(c_{2j-1}^\dagger c_{2j} + c_{2j}^\dagger c_{2j-1} \right) \right. \\
 \left. + i \left(2j + \frac{1}{2} \right) u c_{2j}^\dagger c_{2j} - i \left(2j + \frac{3}{2} \right) u c_{2j+1}^\dagger c_{2j+1} \right], \quad (20)
 \end{aligned}$$

with some unknown proportionality constant. Since we cannot access numerically the full EH of the half-space, in order to test the conjecture in Eq. (20) we study the EH of an interval $[0, \ell]$ in a finite system of length $L \gg \ell$. In analogy with the unitary case, we expect that for a sufficiently large gap, near the endpoints the entanglement Hamiltonian will follow the half-space result in Eq. (20), with a crossover in the middle of the interval, giving rise to the typical triangular shape.

In Fig. 3 we report the results of the numerical calculation of the lattice entanglement Hamiltonian in the gapped phase, for an interval of length $\ell = 100$ in a system of total length $L = 2000$ with periodic boundary conditions. We fix the parameters $v = u = 1$ and we study different gaps by varying the value of w , in particular we take $w = 5, 10$ and 20 . The plots report the ratio between the kernel of the EH, k^A , obtained from Eq. (19) and the one of the Hamiltonian h in Eq. (9) as a function of the lattice site. On the left, in Fig. 3b we report the real part of the nearest-neighbour coupling $k_{j,j+1}^A$, divided by $(-w)$ for j even (circles) and by $(-v)$ for j odd (crosses). Dividing by these coupling constants, we isolate the entanglement temperature, which is expected to follow the triangular shape (see Eq. (20) and discussion below). Indeed we see that, apart from a small crossover region in the center of the interval,

the nearest-neighbour coupling follows the expected behaviour for all values of w that we considered. This behaviour is completely analogous to what observed in Ref. [43] for the dimerised hopping chain. The novel result is reported in the right plot, in Fig. 3b, where we show the staggered imaginary chemical potential $k_{j,j}^A$, divided by u for j even and by $(-u)$ for j odd. Again, the role of this division is to isolate the entanglement temperature, which should agree with the one obtained from the nearest-neighbour coupling. Indeed we observe that, apart from a small oscillation due to finite size effects, the imaginary chemical potential follows the same triangular shape as the nearest-neighbour coupling, as expected from our conjecture in Eq. (20).

As a further check, in Fig. 4 we report the matrix plots of the real (left plot) and of the imaginary parts (right plot) of the single particle EH k^A . According to our conjecture in Eq. (20), the half-space EH does not couple fermions at distances higher than one, similarly to what happens for unitary integrable models in Eq. (8). In the left plot in Fig. 4a, we see that near the endpoints the only non-zero elements of the real part of the EH kernel are the nearest-neighbour couplings $k_{j,j+1}^A$ and $k_{j,j-1}^A$. The higher couplings are non-zero only in a crossover region in the middle of the interval, as expected. This behaviour is again completely analogous to what was observed in Ref. [43] for the dimerised hopping chain. The new results are given by the imaginary part, shown in the right plot in Fig. 4b. We see that also the imaginary part follows the expected behaviour, with only the main diagonal k^A being significantly different from zero near the endpoints. This confirms the validity of our local conjecture in Eq. (20) for the half space EH in the non-Hermitian SSH model. We remark that this is the first observation of a Bisognano-Wichmann like behaviour in a non-Hermitian model.

Before concluding this section, we wish to comment on the proportionality constant in Eq. (20), i.e., the slope of the triangles in Fig. 3. This constant is actually related to the velocity of the excitations in the gapped model. In Ref. [43], the analogous proportionality constant in the dimerised hopping chain was computed analytically using the knowledge of the exact CTM. It would be interesting to obtain analytically the CTM in the non-Hermitian SSH model, which would refine our conjecture (20) for the half-space EH. This computation would not only allow us to predict the slope of the linearly increasing entanglement temperature, but it could also provide a quantitative understanding of the finite size oscillations of the chemical potential in Fig. 3b which are not captured by Eq. (20). This is however a rather involved calculation which goes beyond the scope of this work.

3.2 Entanglement Hamiltonian at the critical point

In this section we study the EH at the critical point $w - v = u$ (green square in Fig. 2). As discussed in Sec. 2, at the critical point and for periodic boundary conditions, the lattice Hamiltonian (9) presents a Jordan block. Then, to treat the system numerically we need to introduce a small twisting of the boundary conditions δ [70, 73]. In all the following discussion we fix $\delta = 10^{-7}$. In full analogy to the study we performed for the gapped phase in Sec. 3.1, we compute numerically the lattice EH kernel k^A using Eq. (19), performing all calculations at high precision. However, at the critical point there is an additional subtlety. In Ref. [70] it was shown that at criticality all eigenvalues ν_j of the correlation matrix are real and lie outside of the interval $[0, 1]$. As a consequence, the matrix appearing inside the logarithm in Eq. (19) has all negative eigenvalues (see also Ref. [73]). This is susceptible to numerical instabilities, giving an imaginary part of the logarithm which (unphysically) oscillates wildly between $+i\pi$ and $-i\pi$. In this work we always fix it to be equal to $+i\pi$.

Before presenting our numerical results for the critical non-Hermitian SSH model, we would like to reiterate what occurs in the case of unitary gapless models. According to Eq. (5), in the vacuum of the CFT describing the continuum limit of a critical model, the entanglement

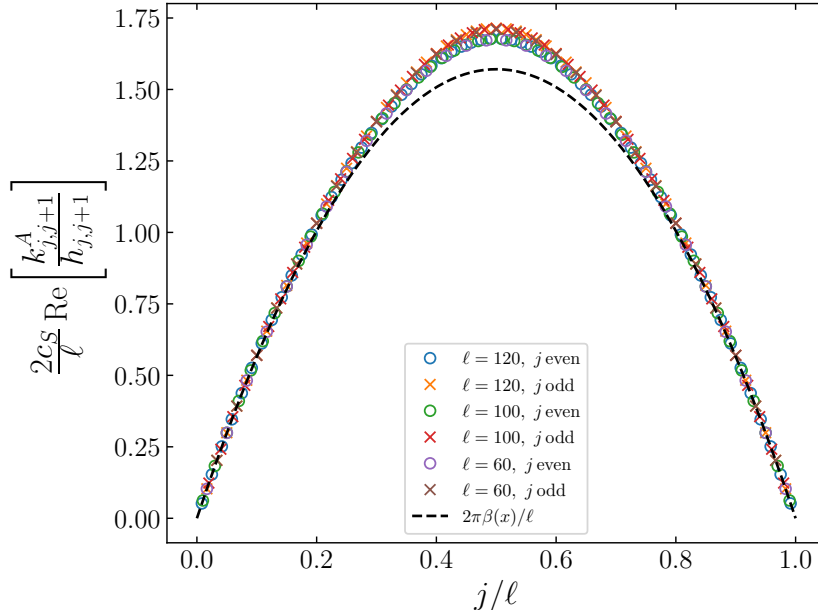


Figure 5: Real part of the ratio of the EH nearest-neighbour coupling $k_{j,j+1}^A$ with the coupling w (v) for j even (odd), rescaled by $2c_S/l$, where l is the length of the interval and c_S is the speed of sound (13). The circles represent even sites and the crosses are odd sites. For all lengths considered we observe a perfect collapse. The black dashed parabola is the field theory prediction for the local temperature $2\pi\beta(x)$ in Eq. (5), divided by l . Near the endpoints of the interval we find a very good agreement between the lattice result and the field theory. The deviation in the middle of the interval is due to the contribution of higher couplings, analogously to what happens in Hermitian lattice models.

Hamiltonian of an interval is proportional to the energy density with a parabolic entanglement temperature $\beta(x)$ [20–23]. One could be tempted to conclude that the EH of an interval in a critical model should be proportional to the critical Hamiltonian density with the parabolic temperature in Eq. (5). This behaviour would in particular imply that all terms of the lattice EH that couple fermions at distances higher than those in the Hamiltonian must be negligible. However, as recognised first in Ref. [89], this is not the case, and the EH contains couplings at arbitrary distances (see also [44–46]). Moreover, when expanding the lattice fermions in the lattice spacing, all these higher couplings contribute to the continuum energy density T_{00} [90, 91]. In Refs. [90–92] it was shown that in order to recover the CFT entanglement temperature $\beta(x)$ in Eq. (5), it is necessary to perform a careful continuum limit which takes into account all of these higher contributions. This limiting procedure has allowed to reconstruct the CFT entanglement Hamiltonian in many systems at criticality, both at finite temperature and in the ground state [90–92] and also in the presence of boundaries [91–93], in inhomogeneous and out-of-equilibrium systems [94] and in higher dimensions [95]. In Refs. [93, 96] it has also been extended to the recently introduced negativity Hamiltonian [97], i.e., the logarithm of the partial transposed density matrix. On the other hand, this limit is highly dependent on the lattice model and, to date, it is only understood in the case of free massless lattice fermions and the harmonic chain.

Considering now the non-Hermitian SSH model, in Figs. 5 and 6, we report the numerical lattice EH, obtained from Eq. (19) with a choice of parameters $w = 1.5$, $v = 1$ and $u = w - v = 0.5$ and different interval lengths $l = 60, 100$ and 120 in a total system of length $L = 2000$. In Fig. 5 we plot the real part of the nearest-neighbour coupling $k_{j,j+1}^A$, divided by $(-w)$ for j even and by $(-v)$ for j odd, analogously to what we have done in the massive case. We further make the quantity dimensionless by multiplying it by $2c_S/l$, where c_S is the speed of

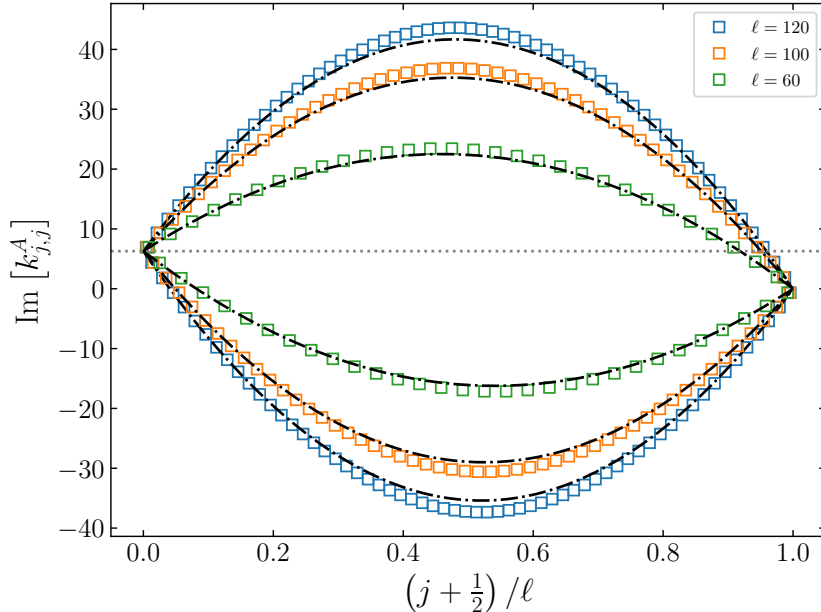


Figure 6: Imaginary chemical potential $k_{j,j}^A$ at criticality $w - v = u$ for different lengths of the interval $\ell = 60, 100$ and 120 . The black dash-dotted curves are reported in Eq. (22) and are obtained as the sum of the naive field theory prediction for the entanglement temperature in Eq. (5) and of the conjectured form of the novel term in Eq. (21). Close to the endpoints we observe a perfect agreement which becomes slightly worse in the middle of the interval.

sound (13) in the critical lattice model. Indeed, notice that if we reintroduce the dimensions, k^A is dimensionless, while w and v have the dimensions of an inverse time. We observe a perfect collapse for all the lengths considered. The black dashed line in Fig. 5 is the parabolic entanglement temperature $2\pi\beta(x)$ for unitary CFTs reported in Eq. (5), divided by the length of the interval ℓ . While near the endpoints we find a good agreement, we see a deviation in the middle of the interval. Similarly to what happens for unitary lattice models, the origin of this discrepancy is the presence of higher couplings which in the continuum limit give contributions to the continuum energy density. We expect that a proper continuum limit should exactly reproduce the parabola in Eq. (5) (as for Hermitian free fermions [90]), but this is beyond our goals.

In Fig. 6 we instead report the staggered imaginary chemical potential (the alternating sign with respect to Fig. 3b is due to not having divided by either u or $(-u)$). This quantity displays the most significant difference with respect to the Hermitian case. For all the lengths ℓ of the interval, at the left endpoint $j/\ell = 0$ the chemical potential takes the value $2\pi i$ (grey dotted line), while at the right one $j/\ell = 1$ it vanishes. Based on this observation, we conjecture that besides the approximate parabolic result, at the critical point appears an additional term of the form

$$\sum_{j=0}^{\ell} \mu_{j,j}^A c_j^\dagger c_j = 2\pi i \sum_{j=0}^{\ell} \left(1 + \frac{(j + \frac{1}{2})}{\ell} \right) c_j^\dagger c_j, \quad (21)$$

i.e., a chemical potential term which interpolates linearly between $2\pi i$ and 0 . We remark that, differently from the parabolic entanglement temperature $\beta(x)$ in Eq. (5), this novel term does not scale with the system size. In order to check Eq. (21), in Fig. 6 we compare the two curves (dash-dotted black lines)

$$\frac{\pi(\pm u)}{c_S} \left(\frac{(\ell - x)x}{\ell} \right) + 2\pi \left(1 - \frac{x}{\ell} \right), \quad (22)$$

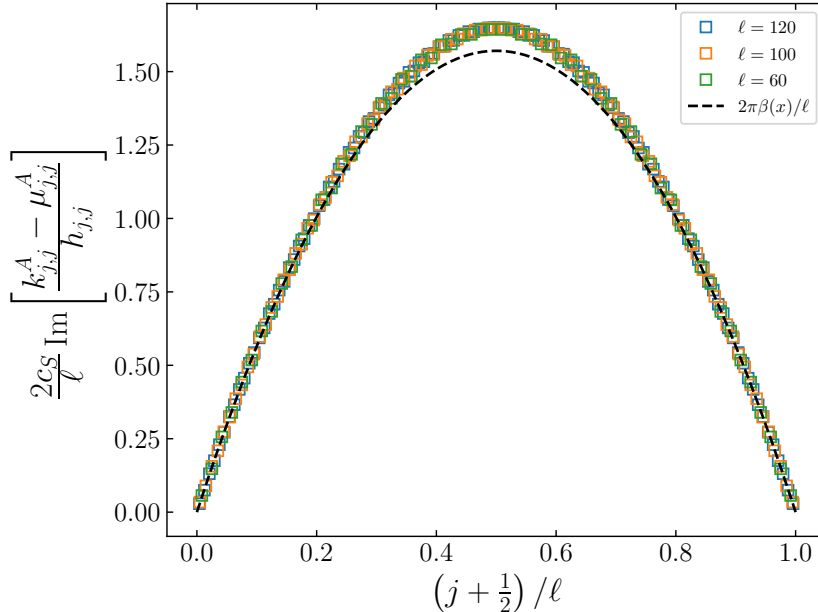


Figure 7: Imaginary part of $(k_{j,j}^A - \mu_{j,j}^A)/h_{j,j}$ (i.e. the difference between the EH the chemical potential and $\mu_{j,j}^A$ in Eq. (21), all in units of $h_{j,j}$), rescaled with $2c_S/\ell$, where c_S is the speed of sound in Eq. (13). We consider intervals of length $\ell = 60, 100$ and 120 in a system of total length $L = 2000$, with parameters $w = 1.5$, $v = 1$ and $u = w - v = 0.5$. For all ℓ , we observe a perfect collapse, suggesting that we have successfully isolated the scaling part. The black dashed curve is the CFT prediction for the entanglement temperature $2\pi\beta$ in Eq. (5) divided by ℓ . Analogously to the nearest-neighbour coupling in Fig. 5, the agreement is perfect at the endpoints and is slightly worse in the middle of the interval, due to the contribution of higher order couplings.

with the imaginary part of the EH chemical potential term for $\ell = 60, 100$ and 120 . Near the endpoints we find a perfect match for all the lengths considered, while the agreement gets slightly worse in the middle of the interval, but still acceptable

To facilitate the comparison, we extract the part of the EH chemical potential that scales with the length of the interval by subtracting the conjectured form $\mu_{j,j}^A$ in Eq. (21) from the numerical result for $k_{j,j}^A$. We then divide by u for j even and by $(-u)$ for j odd to isolate the entanglement temperature and we rescale with $2c_S/\ell$ to make the quantity dimensionless. For all the values of the length considered we observe a perfect collapse, which suggests that the novel non-scaling term $\mu_{j,j}^A$ takes indeed the conjectured form (21). The black dashed curve is again the parabolic CFT prediction for the entanglement temperature in Eq. (5) divided by ℓ . Once again, we have a perfect agreement near the endpoints of the interval, while we observe a deviation in the middle. This deviation is always due to the presence of contributions from higher couplings.

Summing up our finding, recalling from Sec. 2 that the critical point is described by the $c = -2$ bc -ghost CFT, we propose that the continuum limit of the difference $(k^A - \mu^A)$ must reproduce the continuum CFT entanglement Hamiltonian in Eq. (5). Meanwhile, the continuum limit associated with the new chemical potential term μ^A in Eq. (21) will yield

$$\sum_{j=0}^{\ell} \mu_{j,j}^A c_j^\dagger c_j \sim 2\pi i \int_0^\ell dx \left(1 - \frac{x}{\ell}\right) J(x) + \text{irrelevant operators}, \quad (23)$$

where $J(x) = :cb:(x)$ is the ghost number operator. Putting all together, we conjecture that

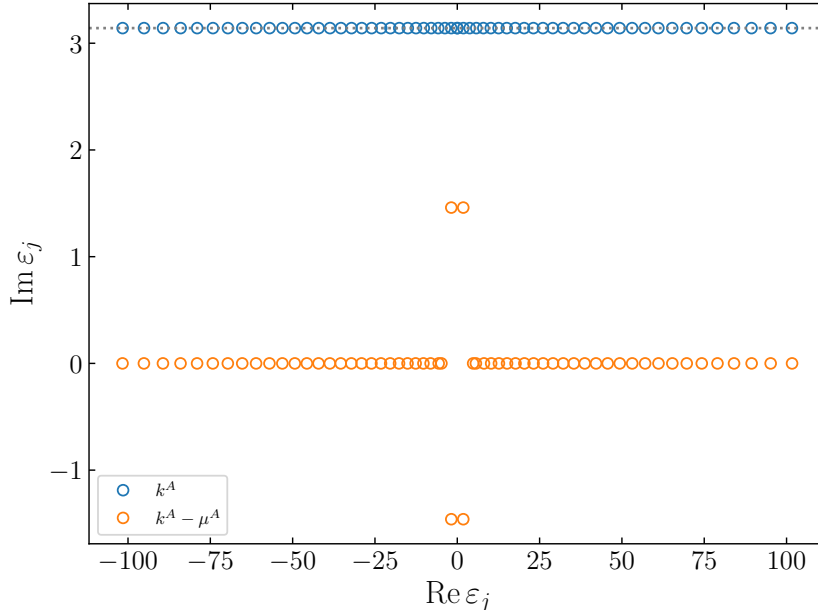


Figure 8: Spectra of the single particle EH k^A (blue) and of the difference $(k^A - \mu^A)$ (orange), where μ^A is given by Eq. (21). The data are for an interval of length $\ell = 120$, in a system of size $L = 2000$, and couplings $w = 1.5$, $v = 1$ and $u = w - v = 0.5$. All eigenvalues of the EH have imaginary part equal to π (gray dotted line). Subtracting μ^A has the net effect of making almost all the eigenvalues real.

the EH of the $c = -2$ bc -ghost CFT would take the form

$$K_A = \int_0^\ell dx \frac{x(\ell-x)}{\ell} T_{00}(x) + 2\pi i \int_0^\ell dx \left(1 - \frac{x}{\ell}\right) J(x), \quad (24)$$

which is one of the main results of this paper. Comparing the proposed entanglement Hamiltonian with the result for unitary CFTs in Eq. (5), the main difference is the presence of the imaginary term proportional to the ghost number $J(x)$. Nevertheless, since this term is again the integral of a local operator, our conjecture (24) retains a local structure. Notice that, since the conformal dimension of the ghost number operator $J(x)$ is $\Delta_J = 1$, the local weight $(1 - x/\ell)$ is dimensionless and it does not scale with the system size, as we observed on the lattice.

In order to understand the role played by the term μ^A in Eq. (21), in Fig. 8 we compare the single particle entanglement spectrum, i.e., the eigenvalues of k^A , with the eigenvalues of the matrix $(k^A - \mu^A)$. All the eigenvalues ε_j of the single-particle entanglement Hamiltonian (blue circles) possess an imaginary part equal to π , a feature previously identified in Ref. [73]. As already mentioned, this imaginary part is due to the fact that the eigenvalues ν_j of the correlation matrix all belong to $(-\infty, 0) \cup (1, +\infty)$, which, using Eq. (19), leads to [73]

$$\varepsilon_j = \log \left| \frac{1 - \nu_j}{\nu_j} \right| + i\pi. \quad (25)$$

As discussed in Sec. 2.2, the impact of the imaginary part in Eq. (25) on the many-body spectrum of the reduced density matrix is to impart an alternating sign to the eigenvalues of ρ_A depending on the charge sector, i.e., the number of ghosts, according to [73]

$$\rho_A = (-1)^{Q_A - \langle Q_A \rangle} |\rho_A|, \quad (26)$$

which in turn is responsible for the negative sign of the entanglement entropy. On the other hand, in Fig. 8 we see that the eigenvalues of $(k^A - \mu^A)$ (orange circles) are almost all real.

We can therefore argue that the novel operator μ^A in Eq. (21) (and its continuum limit (23) in the bc -ghost CFT) is the one responsible for the alternating sign of the entanglement spectrum. Without the operator μ^A , the reduced density matrix ρ_A would be positive defined and, as a consequence, the entanglement entropy would be positive too.

4 Conclusions

In this work we have studied the ground state entanglement Hamiltonian in the non-Hermitian SSH model, considering the left-right density matrix $\rho = |L\rangle\langle R|$. We studied both the topologically trivial gapped phase and the critical point. In the gapped phase, the entanglement Hamiltonian assumes the typical triangular shape (see Eq. (20) and discussion) that was already observed in Ref. [43] for unitary integrable gapped models. Near the endpoints of the interval, the entanglement temperature grows linearly with the lattice site, according to the half-space prediction in Eq. (20). Remarkably, we observe that the same behaviour is true for the imaginary part of the entanglement Hamiltonian. This is the first example of a lattice Bisognano-Wichmann like behaviour in a non-Hermitian model.

At the critical point, described by the bc -ghost CFT, we find a departure from the parabolic entanglement Hamiltonian in Eq. (5) predicted by the Bisognano-Wichmann theorem for unitary CFTs. In addition to a term proportional to the energy density with a parabolic entanglement temperature, we observe a term proportional to the number operator $c_i^\dagger c_i$ with an imaginary chemical potential interpolating between $2\pi i$ and 0, cf. Eq. (21). This operator has a profound effect on the entanglement spectrum. As depicted in Fig. 8, removing the operator in Eq. (21) ensures that almost all the eigenvalues are real. As discussed in Ref. [73], the imaginary part of the single particle entanglement spectrum in Eq. (25) is responsible for the negativeness of the entanglement entropy. If the operator in Eq. (21) were not present, the entanglement entropy would be positive. Based on these results, we formulate a conjecture given by Eq. (24) for the entanglement Hamiltonian in the bc -ghost CFT. Such a conjecture consists of a term analogous to the Bisognano-Wichmann EH in Eq. (5) and of an imaginary chemical potential term proportional to the ghost number $J(x)$.

This paper paves the way for future investigations into the entanglement Hamiltonians of non-Hermitian models. Three open problems emerges very naturally. Firstly, in the gapped phase, it would be interesting to derive analytically the corner transfer matrix. As discussed in Sec. 3.1, this would determine the slope of the triangular entanglement temperature in Fig. 3 and could validate the lattice Bisognano-Wichmann behaviour. Secondly, it is desirable to analytically derive the entanglement Hamiltonian at the critical point, akin to the work done for free massless fermions in Ref. [25]. Thirdly, the robustness of our findings remains uncertain, such as whether the conjectured form of the entanglement Hamiltonian withstands the presence of relevant interactions. Other unexplored research directions include understanding the EH for non-Hermitian systems that lack a real Hamiltonian spectrum.

Acknowledgements

We are grateful to G. Di Giulio and I. Peschel for useful discussions. The authors acknowledge support from ERC under Consolidator grant number 771536 (NEMO).

References

- [1] M. A. Nielsen and I. L. Chuang, *Quantum Computation and Quantum Information*. Cambridge University Press, Cambridge, 2012.

- [2] T. Nishioka, S. Ryu, and T. Takayanagi, *Holographic Entanglement Entropy: An Overview*, *J. Phys. A* **42** (2009) 504008, [arXiv:0905.0932](#).
- [3] L. Amico, R. Fazio, A. Osterloh, and V. Vedral, *Entanglement in many-body systems*, *Rev. Mod. Phys.* **80** (2008) 517, [arXiv:quant-ph/0703044](#).
- [4] P. Calabrese, J. Cardy, and B. Doyon, *Entanglement entropy in extended quantum systems*, *J. Phys. A* **42** (2009) 500301.
- [5] J. Eisert, M. Cramer, and M. B. Plenio, *Area laws for the entanglement entropy - a review*, *Rev. Mod. Phys.* **82** (2010) 277, [arXiv:0808.3773](#).
- [6] N. Laflorencie, *Quantum entanglement in condensed matter systems*, *Phys. Rept.* **646** (2016) 1, [arXiv:1512.03388](#).
- [7] P. Calabrese and J. L. Cardy, *Entanglement entropy and quantum field theory*, *J. Stat. Mech.* (2004) P06002, [arXiv:hep-th/0405152](#).
- [8] P. Calabrese and J. Cardy, *Entanglement entropy and conformal field theory*, *J. Phys. A* **42** (2009) 504005, [arXiv:0905.4013](#).
- [9] H. Li and F. Haldane, *Entanglement Spectrum as a Generalization of Entanglement Entropy: Identification of Topological Order in Non-Abelian Fractional Quantum Hall Effect States*, *Phys. Rev. Lett.* **101** (2008) 010504, [arXiv:0805.0332](#).
- [10] P. Calabrese and A. Lefevre, *Entanglement spectrum in one-dimensional systems*, *Phys. Rev. A* **78** (2008) 032329, [arXiv:0806.3059](#).
- [11] V. Alba, P. Calabrese, and E. Tonni, *Entanglement spectrum degeneracy and the Cardy formula in 1+1 dimensional conformal field theories*, *J. Phys. A* **51** (2018) 024001, [arXiv:1707.07532](#).
- [12] R. Haag, *Local Quantum Physics*. Theoretical and Mathematical Physics. Springer, Berlin, 1996.
- [13] E. Witten, *APS Medal for Exceptional Achievement in Research: Invited article on entanglement properties of quantum field theory*, *Rev. Mod. Phys.* **90** (2018) 045003, [arXiv:1803.04993](#).
- [14] M. Dalmonte, V. Eisler, M. Falconi, and B. Vermersch, *Entanglement Hamiltonians: From Field Theory to Lattice Models and Experiments*, *Annalen Phys.* **534** (2022) 2200064, [arXiv:2202.05045](#).
- [15] J. J. Bisognano and E. H. Wichmann, *On the Duality Condition for a Hermitian Scalar Field*, *J. Math. Phys.* **16** (1975) 985.
- [16] J. J. Bisognano and E. H. Wichmann, *On the Duality Condition for Quantum Fields*, *J. Math. Phys.* **17** (1976) 303.
- [17] S. A. Fulling, *Nonuniqueness of canonical field quantization in Riemannian space-time*, *Phys. Rev. D* **7** (1973) 2850.
- [18] P. C. W. Davies, *Scalar particle production in Schwarzschild and Rindler metrics*, *J. Phys. A* **8** (1975) 609.
- [19] W. G. Unruh, *Notes on black hole evaporation*, *Phys. Rev. D* **14** (1976) 870.

- [20] P. D. Hislop and R. Longo, *Modular Structure of the Local Algebras Associated With the Free Massless Scalar Field Theory*, *Commun. Math. Phys.* **84** (1982) 71.
- [21] H. Casini, M. Huerta, and R. C. Myers, *Towards a derivation of holographic entanglement entropy*, *JHEP* **05** (2011) 036, [arXiv:1102.0440](#).
- [22] G. Wong, I. Klich, L. A. Pando Zayas, and D. Vaman, *Entanglement Temperature and Entanglement Entropy of Excited States*, *JHEP* **12** (2013) 020, [arXiv:1305.3291](#).
- [23] J. Cardy and E. Tonni, *Entanglement hamiltonians in two-dimensional conformal field theory*, *J. Stat. Mech.* (2016) 123103, [arXiv:1608.01283](#).
- [24] G. Sárosi and T. Ugajin, *Modular Hamiltonians of excited states, OPE blocks and emergent bulk fields*, *JHEP* **01** (2018) 012, [arXiv:1705.01486](#).
- [25] H. Casini and M. Huerta, *Reduced density matrix and internal dynamics for multicomponent regions*, *Class. Quant. Grav.* **26** (2009) 185005, [arXiv:0903.5284](#).
- [26] R. E. Arias, H. Casini, M. Huerta, and D. Pontello, *Entropy and modular Hamiltonian for a free chiral scalar in two intervals*, *Phys. Rev. D* **98** (2018) 125008, [arXiv:1809.00026](#).
- [27] M. Dalmonte, B. Vermersch, and P. Zoller, *Quantum Simulation and Spectroscopy of Entanglement Hamiltonians*, *Nature Phys.* **14** (2018) 827, [arXiv:1707.04455](#).
- [28] C. Kokail, R. van Bijnen, A. Elben, B. Vermersch, and P. Zoller, *Entanglement Hamiltonian tomography in quantum simulation*, *Nature Phys.* **17** (2021) 936, [arXiv:2009.09000](#).
- [29] C. Kokail, B. Sundar, T. V. Zache, A. Elben, B. Vermersch, M. Dalmonte, R. van Bijnen, and P. Zoller, *Quantum Variational Learning of the Entanglement Hamiltonian*, *Phys. Rev. Lett.* **127** (2021) 170501, [arXiv:2105.04317](#).
- [30] T. V. Zache, C. Kokail, B. Sundar, and P. Zoller, *Entanglement Spectroscopy and probing the Li-Haldane Conjecture in Topological Quantum Matter*, *Quantum* **6** (2022) 702, [arXiv:2110.03913](#).
- [31] M. K. Joshi, C. Kokail, R. van Bijnen, F. Kranzl, T. V. Zache, R. Blatt, C. F. Roos, and P. Zoller, *Exploring large-scale entanglement in quantum simulation*, *Nature* **624** (2023) 539, [arXiv:2306.00057](#).
- [32] I. Peschel and T. T. Truong, *Corner transfer matrices and conformal invariance*, *Z. Phys. B* **69** (1987) 385.
- [33] B. Davies, *Corner transfer matrices for the Ising model*, *Physica A* **154** (1988) 1.
- [34] T. T. Truong and I. Peschel, *Diagonalisation of finite-size corner transfer matrices and related spin chains*, *Z. Phys. B* **75** (1989) 119.
- [35] I. Peschel, M. Kaulke, and Ö. Legeza, *Density-matrix spectra for integrable models*, *Ann. Physik (Leipzig)* **8** (1999) 153.
- [36] B. Davies, *On the spectrum of six-vertex corner transfer matrices*, *Physica A* **159** (1989) 171.
- [37] H. Frahm and H. B. Thacker, *Corner transfer matrix eigenstates for the six vertex model*, *J. Phys. A* **24** (1991) 5587.

- [38] M. G. Tetel'man, *Lorentz group for two-dimensional integrable lattice systems*, *Sov. Phys. JETP* **55** (1982) 306.
- [39] H. B. Thacker, *Corner Transfer Matrices and Lorentz Invariance on a Lattice*, *Physica D* **18** (1986) 348.
- [40] E. Ercolessi, S. Evangelisti, and F. Ravanini, *Exact entanglement entropy of the XYZ model and its sine-Gordon limit*, *Phys. Lett. A* **374** (2010) 2101, [arXiv:0905.4000](#).
- [41] I. Peschel and T. T. Truong, *Corner Transfer Matrices for the Gaussian Model*, *Ann. Physik (Leipzig)* **48** (1991) 185.
- [42] I. Peschel and M.-C. Chung, *Density matrices for a chain of oscillators*, *J. Phys. A* **32** (1999) 8419, [arXiv:cond-mat/9906224](#).
- [43] V. Eisler, G. Di Giulio, E. Tonni, and I. Peschel, *Entanglement Hamiltonians for non-critical quantum chains*, *J. Stat. Mech.* (2020) 103102, [arXiv:2007.01804](#).
- [44] G. Giudici, T. Mendes-Santos, P. Calabrese, and M. Dalmonte, *Entanglement Hamiltonians of lattice models via the Bisognano-Wichmann theorem*, *Phys. Rev. B* **98** (2018) 134403, [arXiv:1807.01322](#).
- [45] T. Mendes-Santos, G. Giudici, M. Dalmonte, and M. A. Rajabpour, *Entanglement Hamiltonian of quantum critical chains and conformal field theories*, *Phys. Rev. B* **100** (2019) 155122, [arXiv:1906.00471](#).
- [46] J. Zhang, P. Calabrese, M. Dalmonte, and M. A. Rajabpour, *Lattice Bisognano-Wichmann modular Hamiltonian in critical quantum spin chains*, *SciPost Phys. Core* **2** (2020) 007, [arXiv:2003.00315](#).
- [47] V. Eisler, *Entanglement Hamiltonian of a nonrelativistic Fermi gas*, [arXiv:2311.16348](#).
- [48] R. J. Baxter, *Exactly solved models in statistical mechanics*. Academic Press, London, 1982.
- [49] R. J. Baxter, *Corner transfer matrices of the eight-vertex model. 1. Low-temperature expansions and conjectured properties*, *J. Statist. Phys.* **15** (1976) 485.
- [50] R. J. Baxter, *Corner transfer matrices of the eight-vertex model. 2. The Ising model case*, *J. Statist. Phys.* **17** (1977) 1.
- [51] T. Nishino and K. Okunishi, *Corner transfer matrix algorithm for classical renormalization group*, *J. Phys. Soc. Japan* **66** (1997) 3040, [arXiv:cond-mat/9705072](#).
- [52] H. Itoyama and H. B. Thacker, *Lattice Virasoro Algebra and Corner Transfer Matrices in the Baxter Eight Vertex Model*, *Phys. Rev. Lett.* **58** (1987) 1395.
- [53] H. B. Thacker and H. Itoyama, *Integrability, Conformal Symmetry, and Noncritical Virasoro Algebras*, *Nucl. Phys. B Proc. Suppl.* **5** (1988) 9.
- [54] H. Itoyama and H. B. Thacker, *Integrability and Virasoro Symmetry of the Noncritical Baxter-Ising Model*, *Nucl. Phys. B* **320** (1989) 541.
- [55] N. Moiseyev, *Non-Hermitian Quantum Mechanics*. Cambridge University Press, Cambridge, 2011.

- [56] Y. Ashida, Z. Gong, and M. Ueda, *Non-Hermitian physics*, *Adv. Phys.* **69** (2021) 249, [arXiv:2006.01837](#).
- [57] C. M. Bender and S. Boettcher, *Real spectra in nonHermitian Hamiltonians having PT symmetry*, *Phys. Rev. Lett.* **80** (1998) 5243, [arXiv:physics/9712001](#).
- [58] C. M. Bender, *PT-symmetric quantum theory*, *J. Phys. Conf. Ser.* **631** (2015) 012002.
- [59] R. El-Ganainy, K. G. Makris, M. Khajavikhan, Z. H. Musslimani, S. Rotter, and D. N. Christodoulides, *Non-Hermitian physics and PT symmetry*, *Nature Phys.* **14** (2018) 11.
- [60] L. Feng, R. El-Ganainy, and L. Ge, *Non-Hermitian photonics based on parity–time symmetry*, *Nature Photon.* **11** (2017) 752.
- [61] M.-A. Miri and A. Alù, *Exceptional points in optics and photonics*, *Science* **363** (2019) 6422.
- [62] E. M. Graefe, H. J. Korsch, and A. E. Niederle, *Mean-Field Dynamics of a Non-Hermitian Bose-Hubbard Dimer*, *Phys. Rev. Lett.* **101** (2008) 150408, [arXiv:0807.1777](#).
- [63] I. Rotter, *A non-Hermitian Hamilton operator and the physics of open quantum systems*, *J. Phys. A* **42** (2009) 153001.
- [64] M. Müller, S. Diehl, G. Pupillo, and P. Zoller, *Engineered Open Systems and Quantum Simulations with Atoms and Ions*, *Advances in Atomic, Molecular and Optical Physics* **61** (2012) 1.
- [65] S. Gopalakrishnan and M. J. Gullans, *Entanglement and Purification Transitions in Non-Hermitian Quantum Mechanics*, *Phys. Rev. Lett.* **126** (2021) 170503, [arXiv:2012.01435](#).
- [66] A. Biella and M. Schiró, *Many-Body Quantum Zeno Effect and Measurement-Induced Subradiance Transition*, *Quantum* **5** (2021) 528, [arXiv:2011.11620](#).
- [67] X. Turkeshi, A. Biella, R. Fazio, M. Dalmonte, and M. Schiró, *Measurement-induced entanglement transitions in the quantum Ising chain: From infinite to zero clicks*, *Phys. Rev. B* **103** (2021) 224210, [arXiv:2103.09138](#).
- [68] T. Müller, S. Diehl, and M. Buchhold, *Measurement-Induced Dark State Phase Transitions in Long-Ranged Fermion Systems*, *Phys. Rev. Lett.* **128** (2022) 010605, [arXiv:2105.08076](#).
- [69] X. Turkeshi and M. Schiró, *Entanglement and correlation spreading in non-Hermitian spin chains*, *Phys. Rev. B* **107** (2023) L020403, [arXiv:2201.09895](#).
- [70] P.-Y. Chang, J.-S. You, X. Wen, and S. Ryu, *Entanglement spectrum and entropy in topological non-Hermitian systems and nonunitary conformal field theory*, *Phys. Rev. Res.* **2** (2020) 033069, [arXiv:1909.01346](#).
- [71] C. Holzhey, F. Larsen, and F. Wilczek, *Geometric and renormalized entropy in conformal field theory*, *Nucl. Phys. B* **424** (1994) 443, [arXiv:hep-th/9403108](#).
- [72] Y.-T. Tu, Y.-C. Tzeng, and P.-Y. Chang, *Rényi entropies and negative central charges in non-Hermitian quantum systems*, *SciPost Phys.* **12** (2022) 194, [arXiv:2107.13006](#).
- [73] M. Fossati, F. Ares, and P. Calabrese, *Symmetry-resolved entanglement in critical non-Hermitian systems*, *Phys. Rev. B* **107** (2023) 205153, [arXiv:2303.05232](#).

- [74] S. Lieu, *Topological phases in the non-Hermitian Su-Schrieffer-Heeger model*, *Phys. Rev. B* **97** (2018) 045106, [arXiv:1709.03788](#).
- [75] D. Friedan, E. J. Martinec, and S. H. Shenker, *Conformal Invariance, Supersymmetry and String Theory*, *Nucl. Phys. B* **271** (1986) 93.
- [76] S. Guruswamy and A. W. W. Ludwig, *Relating $c < 0$ and $c > 0$ conformal field theories*, *Nucl. Phys. B* **519** (1998) 661, [arXiv:hep-th/9612172](#).
- [77] H. G. Kausch, *Curiosities at $c = -2$* , [arXiv:hep-th/9510149](#).
- [78] H. G. Kausch, *Symplectic fermions*, *Nucl. Phys. B* **583** (2000) 513, [arXiv:hep-th/0003029](#).
- [79] P. Di Francesco, P. Mathieu, and D. Senechal, *Conformal Field Theory*. Graduate Texts in Contemporary Physics. Springer-Verlag, New York, 1997.
- [80] D. C. Brody, *Biorthogonal quantum mechanics*, *J. Phys. A* **47** (2013) 035305, [arXiv:arXiv:1308.2609](#).
- [81] R. Couvreur, J. L. Jacobsen, and H. Saleur, *Entanglement in nonunitary quantum critical spin chains*, *Phys. Rev. Lett.* **119** (2017) 040601, [arXiv:1611.08506](#).
- [82] T. Dupic, B. Estienne, and Y. Ikhlef, *Entanglement entropies of minimal models from null-vectors*, *SciPost Phys.* **4** (2018) 031, [arXiv:1709.09270](#).
- [83] L. Herviou, N. Regnault, and J. H. Bardarson, *Entanglement spectrum and symmetries in non-Hermitian fermionic non-interacting models*, *SciPost Phys.* **7** (2019) 069, [arXiv:1908.09852](#).
- [84] W. Tang, F. Verstraete, and J. Haegeman, *Matrix Product State Fixed Points of Non-Hermitian Transfer Matrices*, [arXiv:2311.18733](#).
- [85] M.-C. Chung and I. Peschel, *Density-matrix spectra of solvable fermionic systems*, *Phys. Rev. B* **64** (2001) 064412, [arXiv:cond-mat/0103301](#).
- [86] I. Peschel, *Calculation of reduced density matrices from correlation functions*, *J. Phys. A* **36** (2003) L205, [arXiv:cond-mat/0212631](#).
- [87] V. Eisler and I. Peschel, *Reduced density matrices and entanglement entropy in free lattice models*, *J. Phys. A* **42** (2009) 504003, [arXiv:0906.1663](#).
- [88] The `mpmath` development team, `mpmath: a Python library for arbitrary-precision floating-point arithmetic (version 1.3.0)`, 2023. <http://mpmath.org/>.
- [89] R. Arias, D. Blanco, H. Casini, and M. Huerta, *Local temperatures and local terms in modular Hamiltonians*, *Phys. Rev. D* **95** (2017) 065005, [arXiv:1611.08517](#).
- [90] V. Eisler, E. Tonni, and I. Peschel, *On the continuum limit of the entanglement Hamiltonian*, *J. Stat. Mech.* (2019) 073101, [arXiv:1902.04474](#).
- [91] V. Eisler, E. Tonni, and I. Peschel, *Local and non-local properties of the entanglement Hamiltonian for two disjoint intervals*, *J. Stat. Mech.* (2022) 083101, [arXiv:2204.03966](#).
- [92] G. Di Giulio and E. Tonni, *On entanglement hamiltonians of an interval in massless harmonic chains*, *J. Stat. Mech.* (2020) 033102, [arXiv:1911.07188](#).

- [93] F. Rottoli, S. Murciano, E. Tonni, and P. Calabrese, *Entanglement and negativity Hamiltonians for the massless Dirac field on the half line*, *J. Stat. Mech.* (2023) 013103, [arXiv:2210.12109](#).
- [94] F. Rottoli, S. Scopa, and P. Calabrese, *Entanglement Hamiltonian during a domain wall melting in the free Fermi chain*, *J. Stat. Mech.* (2022) 063103, [arXiv:2202.04380](#).
- [95] N. Javerzat and E. Tonni, *On the continuum limit of the entanglement Hamiltonian of a sphere for the free massless scalar field*, *JHEP* **02** (2022) 086, [arXiv:2111.05154](#).
- [96] F. Rottoli, S. Murciano, and P. Calabrese, *Finite temperature negativity Hamiltonians of the massless Dirac fermion*, *JHEP* **06** (2023) 139, [arXiv:2304.09906](#).
- [97] S. Murciano, V. Vitale, M. Dalmonte, and P. Calabrese, *Negativity Hamiltonian: An Operator Characterization of Mixed-State Entanglement*, *Phys. Rev. Lett.* **128** (2022) 140502, [arXiv:2201.03989](#).